SPECTRODIRECTIONAL MINNAERT-*K* RETRIEVAL USING CHRIS/PROBA DATA

J. Verrelst [a, *], M.E. Schaepman [a,b], B. Koetz[b], J.G.P.W. Clevers [a]

[a]Centre for Geo-Information, Wageningen UR, Wageningen, The Netherlands – (jochem.verrelst, jan.clevers)@wur.nl
[b]Remote Sensing Laboratories (RSL), Dept. of Geography, University of Zürich, Switzerland – (michael.schaepman, bkoetz)@geo.unizh.ch

KEY WORDS: Minnaert-*k*, RPV model, reflectance anisotropy, forest cover density, snow , CHRIS

ABSTRACT:

This work uncovers the spectral trajectory of the unique structurally-related information content that is embedded in the angular domain of multi-angular remote sensing data. CHRIS (Compact High Resolution Imaging Spectrometer) mounted onboard the PROBA (Project for On-board Autonomy) spacecraft is capable of sampling terrestrial reflectance anisotropy over the visible/near-infrared region of the electromagnetic spectrum with high spatial resolution. The spectral anisotropic behavior of an Alpine coniferous forest during wintertime in relation to forest cover density was investigated using the Minnaert-*k* parameter of the Rahman-Pinty-Verstraete (RPV) model. Although earlier studies have demonstrated that it is possible to use Minnaert-*k* as a proxy for characterizing surface heterogeneity at subpixel scale, its spectral dependency has not yet been fully assessed. Minnaert-*k* parameter retrievals over the full spectral domain of CHRIS data revealed that a turnover from bell-shaped to bowl-shaped anisotropic reflectance patterns occurs when entering the red edge. Specifically, analysis of the underlying dynamics revealed that forest cover density controls the spectral location where this turnover takes place. Due to the bright snow background situation the 773 nm spectral band of CHRIS yielded Minnaert-*k* values that were best related to forest cover density. In this region, medium forest cover densities (40-70%) led to bell-shaped anisotropy patterns, while either sparse canopy covers or dense canopy covers led to bowl-shaped reflectance anisotropy patterns.

1. INTRODUCTION

Reflectance anisotropy of the scattered radiation field of boreal and Alpine forests under winter conditions depends on the wavelength and the proportions of snow and plant cover that are seen by a sensor. These proportions are a function of illumination and viewing angle, topography and structural canopy properties such as tree density, canopy geometry and gap fraction. Since the last two decades, various studies have documented that reflectance anisotropy data encapsulate information about canopy structure at sub-pixel scale (e.g., Diner *et al.,* 1999; Sandmeier and Deering, 1999). Yet it was only with the advent of multi-angular Earth observing sensors and the development of surface reflectance models that physically-based attempts were undertaken to retrieve canopy characteristics from multi-angular reflectance data (e.g., Canisius and Chen, 2007).

Amongst surface reflectance models, the Rahman–Pinty–Verstraete (RPV) semi-empirical parametric model (Rahman *et al.,* 1993) is particularly suitable for estimating reflectance anisotropy because it simulates the bidirectional reflectance distribution function (BRDF) of an arbitrary land surface by using only four parameters. The model is based on simple physical principles and is able to decompose a scattered radiation field of a terrestrial surface as expressed by the bi-directional reflectance factor (BRF) into an amplitude component and a directional component that describes the degree of anisotropy in the scattered radiation field. The angular field is further decomposed into three parameters: a parameter that controls the degree of forward and backward scattering regimes, a parameter that accounts for the hot-spot effect, and a Minnaert function *k* parameter that controls the curvature (e.g. the degree of convexity or concavity) of the reflectance function. Hence, decomposition of the BRF field into one of these parameters results into a newly derived data set that is based on the anisotropy dimension rather than the spectral dimension of the BRF field, and may be mapped and interpreted in its own right. Specifically, the *k* parameter has been shown to better identify canopy structure and heterogeneity at the subpixel scale than is feasible on the basis of spectral measurements only (Pinty *et al.,* 2002; Widlowski *et al.,* 2004).

In 2001 the European Space Agency (ESA) launched the experimental satellite sensor CHRIS (Compact High Resolution Imaging Spectrometer) onboard the PROBA (Project for On-board Autonomy) spacecraft. The hyperspectral instrument captures quasi-instantaneously a series of five angular images at a high spatial resolution (~18 m) as well as at high spectral resolution of a terrestrial surface during the same orbit. Depending on the mode, CHRIS is capable of sampling the anisotropy of the reflected solar radiation field in up to 62 narrow spectral bands over the visible/near-infrared regions (VNIR) of the electromagnetic spectrum (400-1050 nm). Such capacity of sampling the surface-leaving reflectance anisotropy at high spatial and spectral resolution makes CHRIS currently the most promising optical sensor in space to study the usefulness of multi-angular data for forest cover monitoring.

A set of concurrent multi-angular CHRIS images of an old-growth alpine forest stand that is spatially heterogeneous (Kötz *et al.,* 2004) was acquired during wintertime to assess the performance of the Minnaert-*k* parameter. The observations of CHRIS at a high spatial and spectral resolution on the one hand and the contrasting snow-greenness signal on the other hand enable to explore the spatial and spectral dynamics of Minnaert-*k* to the fullest. This brought us to the following objectives: 1) to evaluate the spectral dependency of the Minnaert-*k* parameter that is retrieved from coniferous stands during wintertime, and 2) to evaluate its underlying wavelength-dependent biophysical meaning

* Corresponding author.

1.1 Biophysical interpretation of Minnaert-*k*

Although the RPV model does not handle the radiative properties of the surface explicitly, it may provide valuable material for analyzing the anisotropic spectral behavior of a forest at stand level. The RPV model splits the BRF field into a scalar amplitude component and the associated angular field describing the anisotropy of the surface, that is:

$$BRF(z,\Omega_0,\Omega,\rho_0,k,\Theta,\rho_c) = \rho_0\breve{\rho}(z,\Omega_0,\Omega,k,\Theta,\rho_c) \quad (1)$$

where z represents the amplitude of the BRF measurement, and Ω_0 and Ω represent the direction of incoming and outgoing radiation, respectively. The angular field is a function of a Minnaert-k parameter that controls the bowl or bell-shape, the Θ parameter controls the degree of forward and backward scattering regimes and ρ_c accounts for the hot-spot effect. The parameter k in the modified version of the Minnaert's function has been found of particular interest since it quantifies the degree by which the angular variations in the BRF pattern resemble a concave or convex pattern. It has been proven that under favorable conditions of illumination and background brightness, the angular pattern is largely controlled by the physical properties and geometrical arrangements of the plant elements that constitute the terrestrial surfaces (Pinty *et al.,* 2002). This means that the anisotropic signature as derived from one single wavelength of a vegetated surface can be diagnostic for structural surface properties, given that sufficient spectral contrast between the (darker) overstory and (brighter) background exists.

Coniferous forests are commonly known to appear darker than deciduous forests due to clumping of needles into shoots and the relatively high absorption rate of needles. In coniferous stands at wintertime the following situations can occur:

- Surfaces that are brighter at large oblique viewing angles in forward and backward scattering directions, which is common for more homogeneous surface covers leads to a concave or 'bowl-shape' reflectance anisotropy. Bowl-shaped anisotropy patterns result into k values smaller than 1 when analyzed with the RPV model.
- Conversely, surfaces that are brighter at nadir viewing angle than at oblique viewing angles, which is typical for open canopies, leads to the inverse pattern, that is a convex or 'bell-shape' reflectance anisotropy. Bell-shaped anisotropy patterns result into k values greater than 1.

The Minnaert-k can thus essentially be used as a proxy for canopy heterogeneity simply based on canopy closure and fluctuations in the amount of scattering and absorbing material at one specific wavelength. What is left to be done is evaluating the parameter as a structurally-related proxy over the full spectral domain.

1.2 Test site

An Alpine valley, the Ofenpass valley, located in the Swiss National Park (SNP), South East Switzerland (10°13′48″E/ 46°39′45″N), was chosen as test site. The Ofenpass represents a dry inner-alpine valley with rather limited precipitation (900–1100 mm/a) at an average altitude of about 1900 masl. Two subalpine ecosystems being a coniferous old-growth forest and a meadow dominate the south-facing slope. The forest is largely dominated by mountain pine (*Pinus Montana* spp. *arborea*) and some stone pine (*Pinus cembra*) tree species. These forest stands can be classified as woodland associations of the *Erico-Pinetum mugo* and are typified by relatively open and discontinuous stands. The forests vary in topography, openness, tree clumping, LAI and woodiness. The south-facing valley floor of the Ofenpass valley is considered as core test site.

1.3 CHRIS data

A set of CHRIS mode 5 (land) images were acquired over the SNP site on March 17, 2007, near noon local time (11:34h local time; sun zenith 50°, azimuth 161°) under cloud free conditions. Mode 5 is configured in CHRIS' best spatial resolution (18 m) and spectral resolution (37 narrow bands with bandwidths of 6-33 nm), but it digitizes only half of its swath. The acquisition date was chosen to ensure that a snow carpet is still present while the sun position is already acceptably high at noon. Solar position can be regarded as constant for all five CHRIS Fly-by Zenith Angles (FZA), since the time difference between the first and last recording during the satellite overpass was less than two minutes. In the current along-track pointing configuration, the FZA is equivalent to the nominal view angles (±55°, ±36°, 0°). Due to its narrow field of view (FOV), however, CHRIS is only occasionally able to acquire a target at nominal view angle. PROBA must be tilted at some angle in the across-track direction so that the target area falls within the sensor FOV. This means that the actual observation angles at which the images are acquired may deviate from the nominal view angles. For example, the nominal nadir camera position appeared to be pointed in a forward view zenith angle of +21°.

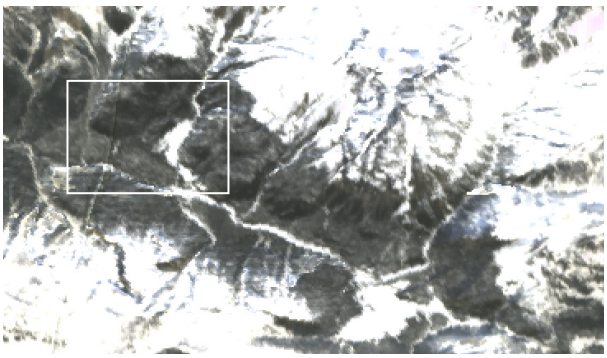

Figure 1: Subset of the geometrically and atmospherically corrected CHRIS nadir scene acquired over the SNP study site on 17 March 2007. The Ofenpass valley stretches from upper left to below right of the image. The square in the upper left corner is considered as the core test site.

The near-nadir image of the Ofenpass valley overpass is depicted in figure 1. The dark parts in the figure exhibit the forest vegetation, the white patch within the dark forest represents a snow-covered meadow. Snow on the branches of the trees had melted, implying that snow-covered forest refers to snow covering the ground surface but not the trees.

Regrettably, as a consequence of the reduced spatial footprint it happened that the backward-pointing -55° view zenith angle just missed the test site. The angular CHRIS scenes of the remaining four images have been corrected following an approach dedicated for rugged, mountainous terrain (Kneubühler *et al.,* 2005) and were subsequently atmospherically corrected. A freely available MODTRAN-based procedure was used that is specifically developed for correcting CHRIS-PROBA images. The method simultaneously derives a set of calibration coefficients and an estimation of water vapour content and aerosol optical thickness from the data themselves (Guanter *et al.,* 2005). All preprocessing efforts finally resulted into geocorrected Hemispherical-Directional-Reflectance-Factor (HDRF) data with a spatial resolution of

18 m. The signal levels were, however, relatively low: a consequence of the relatively low sun zenith angle at the latitude of Switzerland in March. In combination with a terrain elevation of 1900 m this yielded difficulties to MODTRAN in the evaluation of the atmosphere. It resulted into an under-correction of atmospheric effects at the lower wavelengths. Also it resulted into an overcorrection of the water absorption region, which is centered around 940 nm (Guanter *et al.,* 2005). It was therefore decided to remove the first 2 bands (442 and 489 nm) as well as the bands around 940 nm (929, 944 and 959 nm). For all remaining 32 bands the Minnaert-*k* parameter was calculated.

2. METHODS OF DATA ANALYSIS

2.1 Reference map

To enable evaluation of the Minnaert-*k* parameter for its structurally-related information content, it is of importance to identify a structural parameter that has key influence on the reflectance anisotropy that can be used as reference map. A previous study concluded that the horizontal arrangement of the trees and the stand density influences the directional component of the reflectance more than tree height and diameter (Kayitakire and Defourny, 2004). In view of interpreting the Minnaert-*k* parameter as a structurally-related canopy parameter, assessing the relationship with an independent forest cover density map would be the most logical choice. Since illuminated snow and conifer tree crowns are spectrally highly separable, a forest cover density map was generated from the spectral dimension of the CHRIS data set by applying spectral linear unmixing. Spectral mixture analysis was developed to decompose image pixels into their pure constituents, which under winter conditions is a vegetation and a snow signature. As such, the reflectance at pixel level can be described by a spectral mixture model in which a mixed spectrum is represented as a linear combination of pure spectra:

$$R(\lambda)_{pixel} = \mathrm{f}_{\mathrm{vegetation}} R(\lambda)_{\mathrm{vegetation}} + \mathrm{f}_{\mathrm{snow}} R(\lambda)_{\mathrm{snow}} \quad (2)$$

$$\text{and, } \mathrm{f}_{\mathrm{vegetation}} + \mathrm{f}_{\mathrm{snow}} = 1 , \quad (3)$$

where $\mathrm{f}_{\mathrm{vegetation}}$ and $\mathrm{f}_{\mathrm{snow}}$ are the fractions of vegetation and snow respectively, in the pixel studied, and $R(\lambda)$ is the reflectance of each land-cover endmember at wavelength λ. Thereby, the unmixing was forced to be fully constrained (Eq. 3). This guaranteed a physical interpretation of the results since the fractions sum up to 1 and all the fractions are positive. The full spectral domain (without the removed bands) was used to unmix the near-nadir image into these two basic components. Note that linear unmixing quantified the subpixel spectral contributions of overlying canopy and underlying snow cover proportions on the basis of mono-angular, near-nadir spectral measurements.

3. RESULTS AND DISCUSSION

Maps of Minnaert-*k* retrievals were generated for each wavelength to analyze the spatial anisotropic reflectance patterns at landscape level. Six of these maps are shown in figure 2. The excessive blue coloring in the shorter wavelengths, indicates an enhanced (near-) nadir scattering, while excessive red coloring in the longer wavelengths indicates an enhanced oblique scattering. The series of Minnaert-*k* maps show that anisotropy patterns shift from predominantly bell-shaped patterns (k >1.0; in blue color tones) at the shorter wavelengths towards predominantly bowl-shaped patterns (k <1.0; in red color tones) at the longer wavelengths. What these maps also suggest is that largest variability of bell and bowl shapes is located in the red edge (e.g., see the 706 nm map). In the 706 nm map spatial patches of bell-shape and bowl-shape anisotropy patterns emerged that seems to be related to sub-pixel surface cover. The homogeneous non-forested pixels (meadow) exhibit pronounced bowl-shaped reflectance patterns, while there is a fair amount of Minnaert-*k* variability over the forest vegetation, suggesting a relationship with forest structure at sub-pixel scale.

Figure 3 presents the spectral trajectory of the k values averaged for the study site whereby a linear trend emerged. This trend underlines the strong spectral dependency of the Minnaert-*k* parameter. In the visible region bell-shaped reflectance anisotropy patterns dominate (k > 1.0); the bright background controls the reflectance of the entire scene at smaller zenith angles (e.g. near-nadir) while the absorbing properties of the coniferous trees control the reflectance at larger zenith angles.

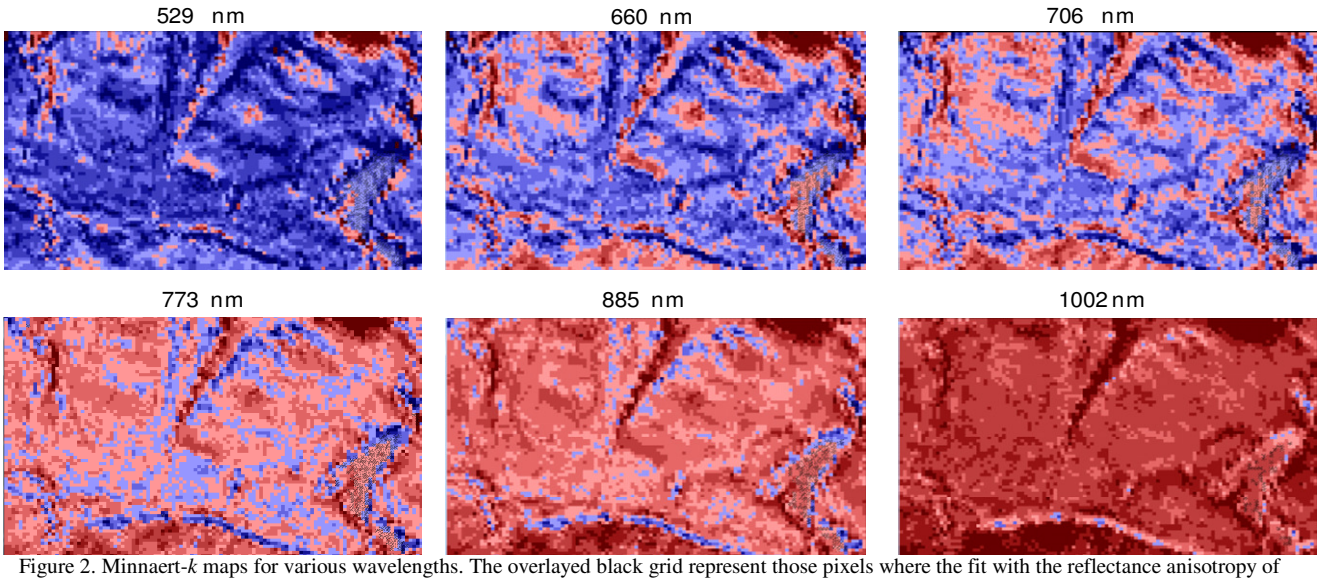

Figure 2. Minnaert-*k* maps for various wavelengths. The overlayed black grid represent those pixels where the fit with the reflectance anisotropy of the inverted RPV BRF data and the HDRF data was significantly different. The color code ranges from red tones for low k values to blue tones for large k values. (lam= lambertian)

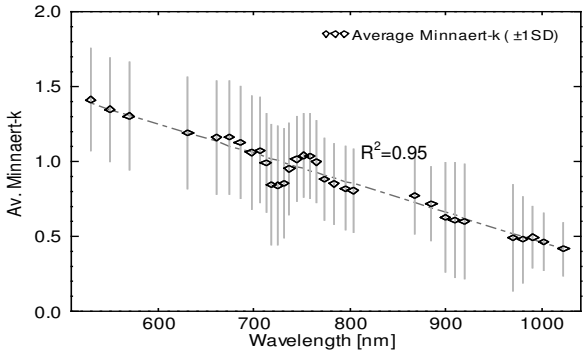

Figure 3: Averaged Minnaert-*k* plus 1SD. A linear trendline was added.

Conversely in the NIR spectral region bowl-shaped reflectance anisotropy patterns dominate (k < 1.0) due to enhanced transmission and multiple scattering processes of NIR radiation throughout the canopy (Sandmeier and Deering, 1999). As a consequence of these multiple scattering processes the spectral contrast between canopy components and background becomes reduced, particularly when moving further in the NIR. It leads to lower k values that vary within a limited numerical range in the NIR, which obstructs the separation of different canopy structures, although some spatially distinct features remain visible. For instance, the riverbank (centre, down) and the edges of the homogeneous snow-covered meadow exhibit a pronounced bell-shape up to the 885 nm map, while at 1002 nm spatial patterns remain visible but k values hardly reach 1. The spatial patterns of contrasting low and high k values can be either explained by extreme topographic features, i.e. by slope and aspect effects, or by subpixel landscape features with extreme spectral contrast, such as road or river banks transecting the vertical-standing coniferous trees.

3.1 Biophysical interpretation

Being aware of a wavelength-dependency of the Minnaert-*k* parameter, the following step involves an analysis of its underlying biophysical meaning. For this analysis CHRIS data of the forest on the south-facing valley floor are used. Although most of the erratic, mountainous terrains are hereby excluded, subtle variations in topography may still lead to target occlusions or larger degrees of anisotropy and thus affect the inversion results. Further interpretations of the retrieved model parameters were therefore restricted to areas with south-facing slopes with a maximal steepness of 10°. This ensured that topographic effects are sufficiently decoupled and that remaining surface anisotropy is solely controlled by vegetation structure and density.

Next, since the curvature of the angular signature heavily depends on the relative share of scattering coming from overstory and background, the independently derived forest cover density map was used as a base map for the biophysical evaluation. The forest cover density map was subsequently stratified into seven forest cover density classes with steps of 10% from 20% onwards. Using forest cover densities as a spatial mask, for each wavelength and forest cover density class the averaged Minnaert-*k* value was calculated (figure 9). The figure shows a systematic, gridded overview of Minnaert-*k* values plotted for the wavelengths recorded by CHRIS along the X-axis and the forest cover densities along the Y-axis. Each grid cell represents thus the averaged Minnaert-*k* value for a specific density class and wavelength. For a few grid cells its associated averaged angular signature is illustrated. The number of pixels per density class is given in a table within figure 9. The table indicates that most of the pixels represent a forest cover density of 60% or higher. Only very few pixels with

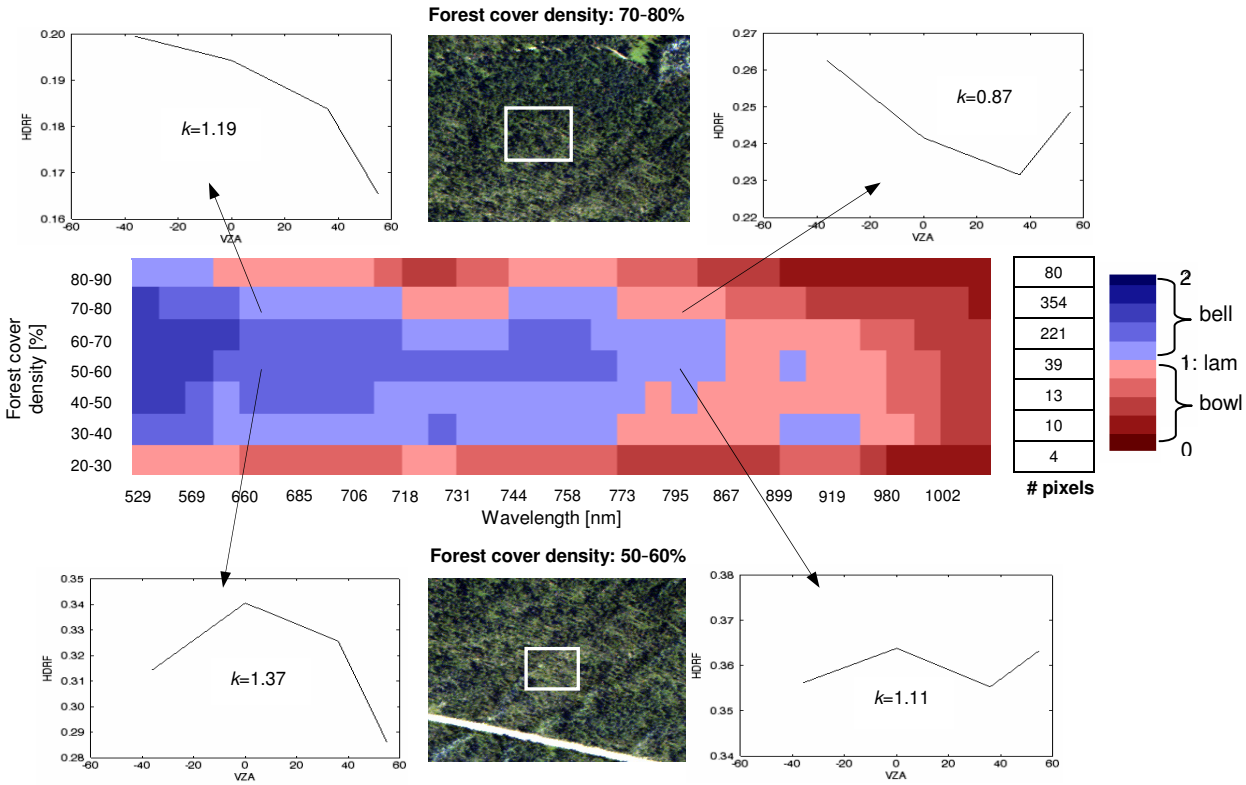

Figure 4: Averaged Minnaert-*k* values as a function of forest cover density and wavelength. The accompanying table represent the number of pixels per forest cover density class. Additional examples of angular signatures are shown. The RGB snapshots are derived from an HRSC camera acquisition in summer 2003. (lam= lambertian)

lower forest cover densities (<40%) are available, potentially weakening the robustness of the results in this range; nevertheless the detected dynamics are sufficiently comprehensive within this figure.

Figure 5 systematically demonstrates that the anisotropic spectral behavior is controlled by the interactions of both forest cover density and wavelength. The underlying radiative transfer dynamics that control the variations of the gridded Minnaert-*k* results are further explained with the help of the example figures illustrated in figure 10. These figures display the spectral trajectories of the averaged anisotropic reflectance signatures for the forest cover densities of 20-30%, 40-50%, 70-80% and 80-90%, respectively. As can be observed from figures 9 and 10, forest cover density essentially determines the relative importance of vegetated overstory and snow cover towards the total top of canopy reflectance, and determines the curvature of the angular signature. For example, it controls whether stand HDRFs are peaking at near-nadir zenith angles (e.g. in case of open canopies) or at higher zenith angles (e.g. in case of closed canopies). Besides, apart from canopy density the curvature of the angular signature, and thus the value of the *k* parameter, is also a function of wavelength. This will be better demonstrated in the next section.

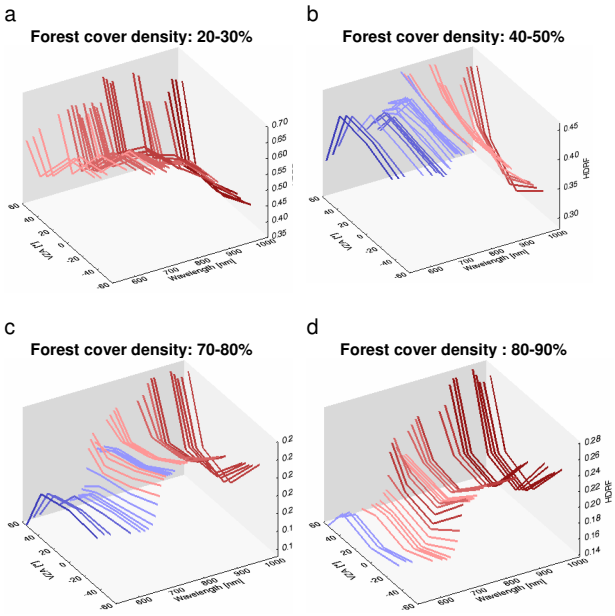

Figure 5: Averaged angular HDRF signatures for 4 forest cover densities (a: 20-30%; b: 40-50%; c: 70-80%; d: 80-90%) with a color depending on the Minnaert-*k* value.

For almost all forest cover densities the signatures at shorter wavelengths are characterized by bell-shaped patterns. Only the extreme sparse forest cover (see figure 5a: 20-30%) gave rise to bowl-shaped anisotropy patterns. In the latter case, the absorptive properties of the sparse tree cover did not exert sufficient influence to alter the typical bowl-shaped reflectance anisotropy into a bell-shaped pattern. This bowl-shape continued merely unchanged throughout the spectral domain. The uncollided forward scattering of snow cover and - from the red edge onwards - some contribution of multiple scattering due to sparse tree cover solely led to enhanced HDRF values at greater zenith angles.

At denser forest covers the contribution of uncollided radiation that is scattered from the bright snow background to the total reflectance is greatest at nadir viewing angle and decreases at greater zenith angles as it becomes obscured by the vertical standing trees, which makes that a bell-shaped reflectance pattern is obtained. Subsequently, when entering into the red edge region a combination of two independent dynamics at subpixel level start to have effect on the top of canopy reflectance anisotropy: 1) a systematic lowering of scattered radiation that exits the snow background due to increased absorption of snow grains, and 2) an increase of multiple scattering processes that govern the dispersion processes of exiting radiation throughout the canopy. The importance of both dynamics is controlled by their respective subpixel proportions, and depending on the spectral contrast between background and canopy it will determine whether and where in the spectral domain a bell-shaped pattern will turn into a bowl-shaped pattern. These dynamics are clearly illustrated for forest cover densities of 40-50% (figure 5b) and 70-80% (figure 5c). Bell-shaped anisotropy signatures are prominently present in the visible spectral region of both strata and even enter the red edge. At a certain wavelength, however, the uncollided, bright yet diminishing snow reflectance is no longer able to provide maximal values at smaller zenith angles. Induced by the enhanced multiple scattering processes throughout the canopy, which start to play an important role from the red edge onwards, high reflectance values at greater zenith angles become dominating: a turnover into a bowl-shape takes place. This turnover will occur quicker at higher tree densities since at higher densities the influence of uncollided radiation from the bright snow background is diminished while the multiple scattering effects are further enhanced. At 40-50% forest cover a bell-shape holds until 773 nm; from there onwards enhanced scattering at larger zenith angles leads to a bowl shape. At denser tree cover (70-80%) the shift from a bell-shape into a bowl-shape takes place more rapidly, i.e. already at the beginning of the red edge (until 712 nm).

Also, it is noteworthy that despite the influence of a medium dense forest cover, the contributing snow reflectance still exerts a strong influence on the spectral anisotropic behavior. This is especially notable for the near-nadir data in the 900 nm region where reflectance values continue to drop.

At even denser forest cover (between 80-90%; figure 9d), the tree crowns are so densely packed that the remaining uncollided radiation from the snow background is hardly able to enforce a bell-shaped pattern. Only in the red spectral range sufficient spectral contrast between the dark canopy and the bright background remains. Yet, once entering the red edge, the predominantly multiple scattering processes throughout the canopy directly outperform the influence of single scattering from the snow layer and shift into a bowl-shaped pattern.

3.2 Applications Minnaert-*k*

In the initial work of Pinty *et al.* (2002) the use of measurements in the red spectral region was advocated, as there the subpixel absorption/reflectance contrast between the vertical-standing, photosynthetically active coniferous trees and the underlying soil cover is maximized. Yet the latter referred to summertime conditions whereby maximal spectral contrast with vegetation is given by a bright bare soil. In a wintertime landscape the influence of the underlying bright snow cover is considerably larger, i.e. significant spectral contrast continues throughout the red edge. This greater spectral contrast led to the turnover from bell to bowl-shapes moving throughout the red edge towards the early NIR. Although the Minnaert-*k* is a semi-empirical parameter, bell-shaped and bowl-shaped reflectance anisotropy are bounded by physical limitations, both by forest cover density as well as by wavelength. For instance, the bell-

shaped pattern dominates throughout the visible and narrows down to medium forest cover densities throughout the red edge. Identification of this distinct bell-shaped pattern for a given overstory canopy and background type may lead to an improved selection of an appropriate wavelength for Minnaert-*k* mapping.

As in the red edge and early NIR region reflectance anisotropy turnovers are taking place as a function of forest cover density, it provides the critical region to characterize stand heterogeneity under winter conditions. Inspection of figure 4 reveals that most promising results appear in the 773 nm region. In this region blue coloring indicates the presence of a heterogeneous surface type such as a forest between 40% and 70% cover. Red color tones indicate the presence of a structurally homogeneous surface such as either a sparse tree cover up to 40% or a dense tree cover with a forest cover over 70%. Moreover, apart from forest cover density the Minnaert-*k* parameter also acts as vertical profiling proxy within a canopy: high *k* values (>1.0, bell-shaped) indicate not only the occurrence of gap effects, but also the occurrence of vertical structures within a pixel. For instance, the depth of the bell-shaped curvature for a given forest cover density will be controlled by tree height; i.e. tall coniferous trees will lead to a more pronounced bell-shaped curvature compared to low-growing plants (e.g. shrubs) because tall coniferous trees obscure the background-leaving radiation into sensor direction already at smaller zenith angles. Conversely, low *k* values (<1.0, bowl-shaped) characterize pixels where a vertical profile is absent. This notion of vertical profiling makes the Minnaert-k parameter more unique than a forest cover density map; it provides a quantitative indicator of 3D heterogeneity at subpixel scale. Research in this direction was initiated by Widlowski *et al.* (2004). By using a ray-tracing radiative transfer model, they attempted to relate the Minnaert-*k* parameter to both tree density and tree height. The relationships found were subsequently tested in real world stand (SNP) using a LiDAR dataset (Koetz *et al.,* 2005). Although multiple solutions did occur for a single *k* value (an example of the well-known ill-posed problem), canopies with heterogeneity in either horizontal or vertical dimension were successfully discriminated from homogeneous canopies.

However, the fact that the red color tones in figure 8 (bowl-shaped anisotropy patterns; $k<1.0$) either represent an open snow-covered surface or a dense forest cover still poses a problem in the interpretation of *k* values. To overcome this problem, an option would be to combine the Minnaert-k map with the spectral dimension of the RPV model (e.g. the amplitude parameter) whereby the dark spectra (vegetation) can be easily discriminated from the bright (snow) spectra. Another option is combining the Minnaert-*k* map with an independently derived forest cover map. Hyperspectral multi-angular CHRIS data are particularly useful for generating both kinds of maps, e.g. by applying linear unmixing in the spectral domain and Minnaert-*k* retrieval in the directional domain. Merging both products may yield subpixel information beyond what is possible from single-source data sets

4. CONCLUSIONS

The European Space Agency's small PROBA satellite holds the only hyperspectral sensor in space (CHRIS) that provides multi-angular measurements. Yet applications in the angular domain of remote sensing data have not been fully developed. This paper links anisotropic reflectance signatures of a forested surface as observed from space with forest 3D-heterogeneity at subpixel scale in the full spectral domain. We used spectrodirectional CHRIS data to elaborate the exploitation of reflectance anisotropy and more specifically addressed the spectral dependency of the Minnaert-*k* parameter. Images of coniferous stands acquired during winter have been found particularly useful to evaluate the underlying biophysical information content that is embedded in the angular domain. For each CHRIS wavelength, the Minnaert-*k* parameter quantified variation in anisotropic reflectance signatures of forest vegetation into a single value, which was compared with an independently derived forest cover density map. A spectral trajectory from predominantly bell-shaped anisotropy patterns in the visible spectral region towards predominantly bowl-shaped anisotropy patterns in the NIR spectral region emerged. Due to the bright underlying snow cover a turnover was found somewhere in the red edge/ early NIR region, whereby its exact spectral position was controlled by forest cover density. The 773 nm spectral region provided Minnaert-*k* values that were comprehensively related to forest cover density. In turn, when the background is less bright than snow cover then the turnover from bell to bowl-shapes is expected to occur earlier in the spectral domain due to a reduced spectral contrast.

5. ACKNOWLEDGEMENT

The work of J. Verrelst was supported through the Dutch SRON GO programme (Grant-No. EO-080).

6. REFERENCES

Canisius, F., & Chen, J.M. (2007). Retrieving forest background reflectance in a boreal region from Multi-angle Imaging SpectroRadiometer (MISR) data. *Remote Sensing of Environment, 107*, 312-321

Diner, D.J., Asner, G.P., Davies, R., Knyazikhin, Y., Schaaf, C.B., Muller, J.P., Nolin, A.W., Stroeve, J., & Pinty, B. (1999). New Directions in Earth Observing: Scientific Applications of Multiangle Remote Sensing. *Bulletin of the Am. Meteorological Society, 80*, 2209

Guanter, L., Alonso, L., & Moreno, J. (2005). A method for the surface reflectance retrieval from PROBA/CHRIS data over land: Application to ESA SPARC campaigns. *Ieee Transactions on Geoscience and Remote Sensing, 43*, 2908-2917

Kayitakire, F., & Defourny, P. (2004). Forest type discrimination using multi-angle hyperspectral data. In, *ESA SP,* 72-84

Kneubühler, M., Koetz, B., Richter, R., Schaepman, M., & Itten, K. (2005). Geometric and radiometric pre-processing of CHRIS/PROBA data over mountainous terrain. In, *ESA SP,* 9-64

Koetz, B., Kneubülhler, M., Widlowski, J.L., Morsdorf, F., Schaepman, M., & Itten, K. (2005). Assessment of canopy structure and heterogeneity from multi-angular CHRIS-PROBA data. *The 9th Int. Symp. on Physical Measurements and Signatures in RS*, 73-78

Rahman, H., Verstraete, M.M., & Pinty, B. (1993). Coupled Surface-Atmosphere Reflectance (Csar) Model .1. Model Description and Inversion on Synthetic Data. *Journal of Geophysical Research-Atmospheres, 98*, 20779-20789

Pinty, B., Widlowski, J.L., Gobron, N., Verstraete, M.M., & Diner, D.J. (2002). Uniqueness of multiangular measurements - Part I: An indicator of subpixel surface heterogeneity from MISR. *Ieee Transactions on Geoscience and Remote Sensing, 40*, 1560-1573

Sandmeier, S., & Deering, D.W. (1999). Structure Analysis and Classification of Boreal Forests Using Airborne Hyperspectral BRDF Data from ASAS. *Remote Sensing of Environment, 69*, 281

Verrelst, J., Schaepman, M.E., Koetz, B., & Kneubühler, M. (2008). Angular sensitivity analysis of vegetation indices derived from CHRIS/PROBA data. *Remote Sensing of Environment, 112*, 2341-2353

Widlowski, J.L., Pinty, B., Gobron, N., Verstraete, M.M., Diner, D.J., & Davis, A.B. (2004). Canopy structure parameters derived from multi-angular remote sensing data for terrestrial carbon studies. *Climatic Change, 67*, 403